Some Aspects of Deformation and Fracture in Carbons

Brian McEnaney,
Materials Research Centre, University of Bath, Bath, BA2 7AY, UK

Introduction

Carbon materials are manufactured in an amazing variety of forms. Some forms have densities and degrees of crystalline perfection that approach that of graphite single crystals while others have highly disordered structures. Most carbon materials contain porosity that can have an adverse effect upon mechanical properties. The ranges of strength and Young's modulus for different carbon materials are represented in Figure 1. Engineering carbon materials such as carbon-carbon composites, pyrocarbons, glassy carbons and polygranular carbons and graphites have bulk densities greater than 1 g cm^{-3}, corresponding to pore volume fractions $V_p < \sim 0.5$. Figure 1 shows that values of Young's modulus and strength for these materials range over three and four orders of magnitude respectively. The normalized strength values, σ_f/E, lie between $\sigma_f/E = 10^{-4}$ and 0.05, Figure 1. The data envelopes for these carbons overlap to some extent with those found for other porous ceramics and engineering composites [1].

Low-density forms of carbon can be manufactured as foams, *e.g.,* by carbonization of phenolic resins. Low-density carbon-bonded carbon fibers can also be produced by adapting paper making technology or by slurry molding of chopped carbon fibers with a resin binder [2]. These low-density forms of carbon can have very high pore volume fractions, $V_p > 0.9$, and correspondingly low values of stiffness and strength, Figure 1, with normalized strengths in the range $\sigma_f/E = 5 \times 10^{-3} - 0.1$. If these low-density forms are included with the other forms of carbon, then both stiffnesses and strength range over six orders of magnitude. This is an illustration of the unique versatility of carbon as a material and its ability to be manufactured in very wide variety of forms.

The remainder of this paper is mainly devoted to work carried out at Bath on some aspects of deformation and fracture of polygranular graphites.

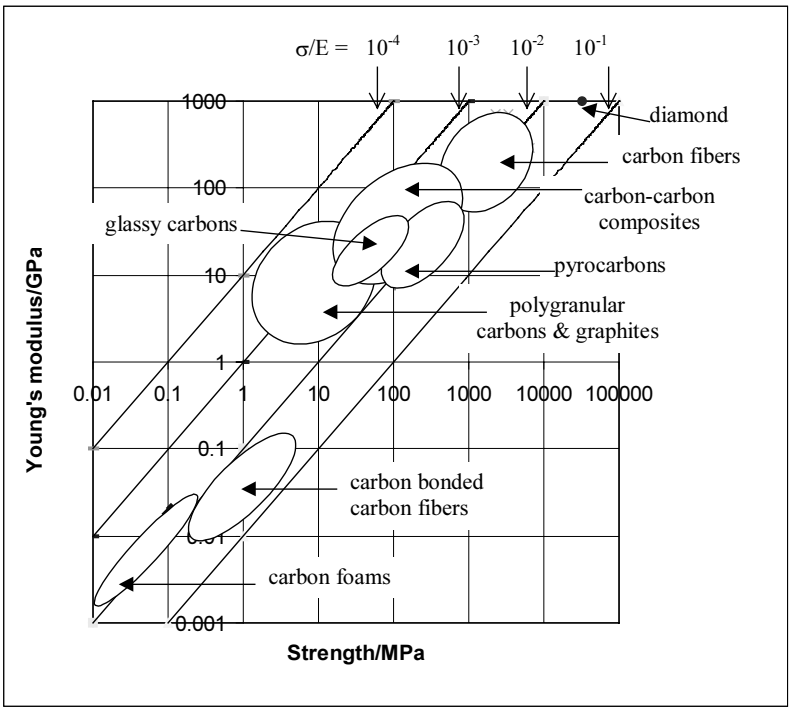

Figure 1. Young's modulus and tensile strengths[a] of some carbon materials.
(a. flexural and compressive strengths for carbon bonded carbon fibers and carbon foams respectively.)

Deformation and Fracture of Polygranular Graphites

The stress-strain response of polygranular graphites is non-linear with the tangent modulus decreasing with increasing load. There is hysteresis on unloading with a residual strain at zero load. Figure 2 shows an example of this behavior for controlled crack growth in a notched graphite specimen subject to cyclic loading and unloading [3]. A rheological model for this type of deformation behavior was proposed by Jenkins [4] in which progressive plastic deformation within filler particles is restrained by the binder phase, which behaves elastically. Plastic deformation within well-graphitised filler grains may include dislocation movement, basal plane shear and cleavage.

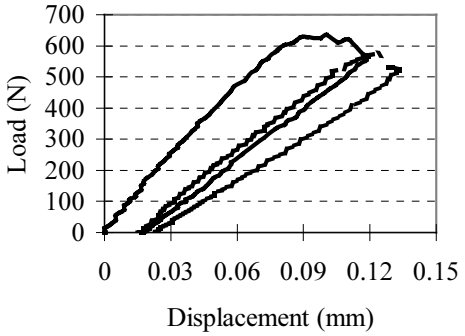

Figure 2. Load-displacement curves for two cyclic loadings of a notched compact tension specimen of IM1-24 graphite [3].

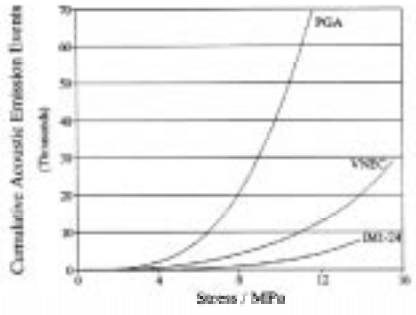

Figure 3. Typical AE response from three nuclear grade polygranular graphites under tensile loading [5].

Abundant microscopical studies have shown for polygranular graphites, stressed in various ways, that microcracking occurs within the filler and binder phases and at filler-binder interfaces. Acoustic emission, AE, during mechanical testing of polygranular graphites shows clear evidence for sub-critical activity [5-8]. Some examples of cumulative AE counts for tensile loading of three nuclear grade graphites are shown in Figure 3 [5]. The much greater extent of AE from PGA graphite can be related to extensive sub-critical cracking as a result of its coarser texture.

Creep and Recovery in Polygranular Graphites

Acoustic emission has also been used at Bath to study creep and recovery processes in stressed polygranular graphites. The effect of cyclic compressive loading of a polygranular graphite on cumulative AE when the time between cycles is zero is shown in Figure 4 [8].

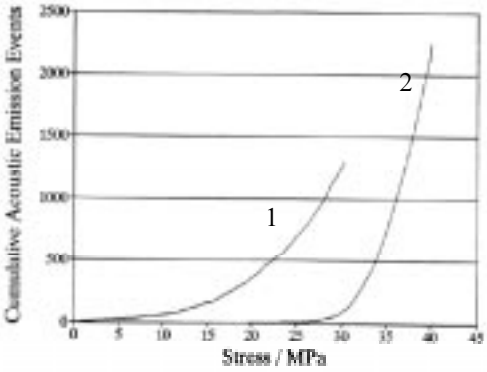

Figure 4. Acoustic emission from IM1-24 graphite subject to cyclic compressive loading when the time between loading is zero minutes [8].

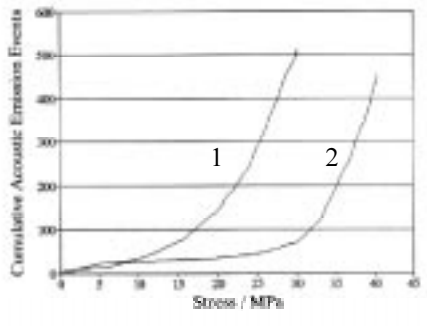

Figure 5. Acoustic emission from IM1-24 graphite subject to cyclic compressive loading when the time between loading is 10^5 minutes [8].

There is clear evidence for a resumption of AE on the second cycle at stresses below the maximum value on the first cycle. This is known as a Felicity effect and it is attributed to recovery processes occurring upon unloading. Earlier

work [9], using less sensitive AE detection equipment, suggested that there was no AE on the second cycle until the previous maximum stress was exceeded - a Kaiser effect. The effect of recovery on AE during cyclic loading is also illustrated in Figure 5, which is the result of a similar experiment to that shown in Figure 4, except that the time between cycles was 10^5 minutes. Here, there is acoustic emission from the start of loading during the second cycle.

Thus there are at least two factors contributing to recovery: (i) recovery during unloading which is perhaps due to some reversal of inter-crystalline shear, and (ii) relaxation of residual strains at zero stress which is a function of time, *i.e.,* a form of creep recovery at room temperature.

Further evidence for room temperature creep of graphite is shown in Figure 6, which presents accumulative AE as a function of time for polygranular graphite specimens subject to constant compressive strain. There is substantial AE associated with the application of the initial compressive stress (24.2 MPa) and further increments of AE, amounting to an additional ~1%, but extending over ~1000 minutes.

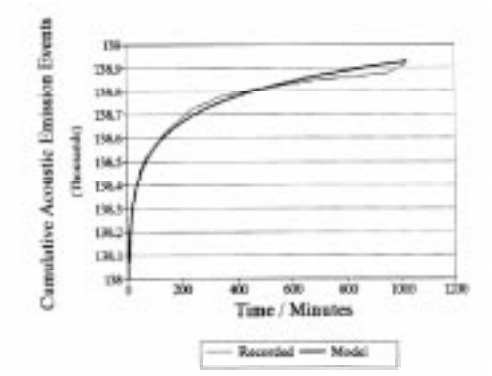

Figure 6. Acoustic emission from IM1-24 graphite subject to compressive strain. Initial stress = 24.2 MPa. Model curve calculated from Equation (3) [8].

Andrew *et al* [10] studied creep of graphites at room temperature and showed that the permanent set on unloading graphites increased logarithmically with time of loading. Davidson and Losty [11] showed for a range of carbons and graphites that at elevated temperatures (1300-2000 ^{o}C) primary creep strain, ε_t, as a function of time, t, could be fitted to a logarithmic expression

$$\varepsilon_t = A + k \log t \,, \qquad (1)$$

where A and k are constants. The instantaneous strain, $A = \sigma/E$, where σ is the applied stress and E is Young's modulus. It is possible to relate the AE response curve in Figure 6 to Equation (1). If each localized creep process consists of abrupt increments of localized creep strain, $\Delta\varepsilon$, and each increment acts as an AE source, then the sum of AE events at time t, ΣN_t, is directly related to the accumulation of creep strain increments

$$\Sigma N_t = f(\Sigma\Delta\varepsilon) = f(\varepsilon_t) \qquad (2)$$

If it is further assumed that secondary creep at ambient temperature is negligible, then the ΣN-time curves for constant strain can be related to Equation (1) thus:

$$\Sigma N_t = \Sigma N_0 + k_{ae} \log t \qquad (3)$$

where ΣN_0 represents the cumulative AE event count due to the instantaneous load at t = 0 and k_{ae} is a constant similar to k in Equation (1). Figure 6 shows that it is possible to fit Equation (6) to the data quite well. A similar result to that in Figure 6 was obtained for AE from a polygranular graphite specimen at zero load after being subjected to a compressive pre-stress, except that the extent of AE was smaller [8].

Toughness of Carbon Materials

Linear elastic fracture mechanics, LEFM, have been applied extensively to polygranular graphites. Values of critical stress intensity factor, K_{Ic}, range from 0.5-1.5 MPa.m$^{0.5}$; similar values of K_{Ic} are found for other porous ceramics and rocks [1]. For medium and coarse textured polygranular graphites, critical flaw sizes, a_c, in the range 0.5-1.5 mm can be estimated from K_{Ic} and the fracture stress, σ_f, using the equation

$$a_c = \frac{(K_{Ic}/\sigma_f)^2}{\pi Y^2} \qquad (4)$$

where Y is a flaw shape correction factor. Critical flaw sizes estimated this way have been related to the dimensions of filler particles or pores or inherent cracks or combinations of these microstructural features [7].

Although extensively used, Linear Elastic Fracture Mechanics are of doubtful validity when applied to polygranular graphites and carbon-carbon composites. For both types of carbon material the stress-strain response is non-linear, *e.g.,* Figure 2. There is structural anisotropy, and the critical defect size is small in relation to the size of the process zone. As a result, elastic-plastic fracture mechanics, EPFM, have been applied to such carbons, since these methodologies can take account of factors such as non-linear stress-strain response and large process zones around the crack tip [12]. Using EPFM, the toughness of materials can be characterized by the crack growth resistance parameter, R/(J m^{-2}), Table 1.

Table 1 shows that diamond and glassy carbons are brittle materials, R < ~20 J m^{-2}), while pyrolytic carbons and polygranular graphites are semi-brittle materials (~20 < R < ~500 J m^{-2}). In the latter case the energy dissipation mechanisms include shear deformation within grains and sub-critical cracking, as discussed above. For cracks propagated perpendicular to lamellae, a woven carbon-carbon composite is a very tough material with values of R that are orders of magnitude higher than those found for the other forms of carbon. However, because of the marked anisotropy of bi-directional carbon-carbons, cracks propagate easily between lamellae, giving a value of R that is similar to fine-textured polygranular graphites.

Table 1. Crack Growth Resistance, R/(Jm^{-2}) of Some Carbon Materials.

Carbon material	**R**
Diamond	13-18
Glassy carbons [a]	12-14
Pyrolytic graphite [b]	38
Fine textured graphite [a]	20-70
Medium textured graphite [a]	120-200
Coarse textured graphite [a]	232-258
Bi-directional woven CC [c]	50000
Bi-directional woven CC [d]	60-95

a. initial R value; b. crack length and width parallel and perpendicular to deposition plane resp.; c. crack length perpendicular to lamellae; d. crack length parallel to lamellae.

Further insights into crack propagation in carbon materials are provided by R-curves, *i.e.,* plots of crack growth resistance as a function of crack extension. Figure 7 shows an R-curve for crack propagation in a compact tension specimen of a nuclear grade, polygranular graphite. There is a rising R-curve in the initial stages of crack extension followed by a plateau region with R ~300 J m^{-2}. The value of R then decreases as the crack approaches the back face of the specimen.

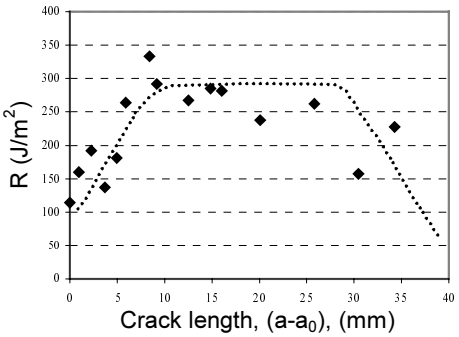

Figure 7. R-curve for crack propagation in a compact tension specimen of IM1-24 graphite [3].

There are two main factors that shield the crack tip from the applied stress and so confer toughness. The first is a process zone ahead of the crack tip in which microcracking and other inelastic processes occur. The second is the development of crack bridging in the wake region behind the crack tip by fragments of graphite. Here, the frictional effects of the crack bridging particles contribute to toughness. Some examples of crack bridging in the crack wake region for a polygranular graphite are shown in Figure 8.

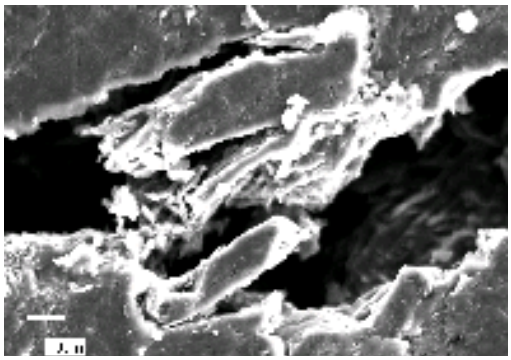

Figure 8. Crack bridging in the wake zone for PGA graphite Magnification bar = 10 μm [3].

The initial, rising R-curve is attributed to the growth of the process zone ahead of the crack tip, and the development of tractions in the crack wake region caused by crack bridging. Recent work at Bath [3] suggests that the process zone ahead of the crack tip develops before crack extension commences, so that the rising part of the R-curve is due almost entirely to growth of crack bridging. The plateau in the R-curve corresponds to crack propagation with a steady state process zone and crack wake region. The usual explanation for the eventual decrease in R is that the contribution to R from process zone activity diminishes as the back face of the specimen is approached.

Rising R-curves of similar form to Figure 7 have been reported for controlled crack growth in carbon-carbons, except that the value of R in the plateau region is in the range 2-4 kJ m^{-2}, reflecting their much greater toughness [13]. Here, the inelastic processes include some of those proposed for the generality of continuous fiber reinforced composites: fiber/matrix interfacial de-bonding ahead of the crack tip and fiber bridging in the wake region. Other factors include frictional resistance to crack opening by intact fibers in the wake region and pull-out of fractured fibers. The substantial energy dissipations associated with these processes lead to the high toughness of carbon-carbons.

Blunt Indentation of Polygranular Graphites

There has been extensive work on the mechanical properties of polygranular graphites subject to conventional stress states: tension, flexure, compression. Also, more limited studies have been made of the response of graphites to multi-axial stresses, creep and fatigue. By contrast, the response of engineering grade graphites to contact stresses has hardly been studied at all. An investigation of blunt indentation of polygranular graphites was undertaken at Bath [14-16]. This was prompted by the possibility of such stresses developing in graphite moderated gas-cooled nuclear reactors in the UK.

The simple experimental apparatus used for this work is shown in Figure 9. A 6 mm diameter tungsten carbide sphere was chosen as the indentor and an Instron testing machine supplied the load. Displacements were measured using an LVDT. Disc shaped graphite specimens 19 mm diameter and 10 mm thick were used. A bonded interface technique was used to study microstructural damage accumulation beneath the indentor. The specimens were cut in half and the cut surface polished to a sub-micron finish. They were then bonded together using cyanoacrylate glue. The indentations were made at the glue line. Afterwards, the two halves of the specimens were separated using a solvent so that the microstructural damage could be inspected.

Figure 9. The Blunt indentation apparatus [14].

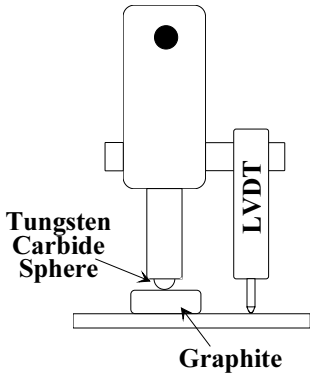

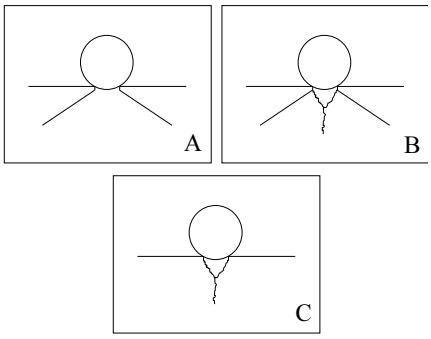

Figure 10. Schematic of indentation fracture of graphite with different textures, A spherical tungsten carbide indenter of diameter 6mm was used. A, Poco ZXF graphite, B, EY306 graphite, C, IM1-24 graphite [15].

The effect of microstructure was investigated using three graphites of different texture: Poco ZXF graphite, a fine grained graphite, particle size ~1 μm; Morganite EY 306, an intermediate textured graphite, particle size ~10 μm; BAEL IM1.24 a Gilsocarbon graphite with a filler particle size of ~500 μm.

The damage accumulation after indentation is shown schematically in Figure 10. Micrographs are shown in Figure 11. Poco graphite ZXF, Figures 10A, 11a, produces a near-classical Hertzian cone crack after indentation, the crack initiates at a surface flaw close to the region of maximum stress and propagates outwards. This

indicates that the graphite behaves as an isotropic continuum under indentation loads, rather like glass. By contrast, the coarse textured IM1-24 graphite, Figures 10C, 11c, shows no evidence for Hertzian cracking. Instead, there is evidence for microcracking in the binder phase induced by shear deformation in the stress field beneath the indentor. There is also evidence for damage due to compression immediately below the indentor. The intermediate textured graphite, EY 306, shows mixed behavior with a Hertzian type cone crack and microcracking beneath the indentor induced by shear and compresion, Figures 10B, 11b.

Acknowledgements. I acknowledge with pleasure and thanks the major contributions to the work described in this paper made by my present and former research students and collaborators: Dr Tim Burchell, Dr Robin Cooke, Dr Mark Hartley, Mr Mike Phillips, Dr Gareth Neighbour, Mr Pierre Ouagne, Dr Ian Pickup. I also acknowledge financial support for this work over the years from what is now British Energy Generation Ltd. and the Engineering and Physical Sciences Research Council of the UK.

References

1. Ashby MF. *Materials selection in mechanical design*. Oxford:Pergamon. 1992: 34-35.
2. Burchell TD. In Burchell TD, editor. *Carbon materials for advanced technologies*. Oxford:Pergamon. 1999:169-204.
3. Ouagne P. PhD thesis, University of Bath, UK, in preparation.
4. Jenkins GM. Philosophical Magazine, 1963;8:903-910.
5. Neighbour GB, McEnaney B, Phillips MG. Carbon, 1992;30:359-364.
6. Burchell TD, Cooke RG, McEnaney B, Pickup, IM. Carbon, 1985;23:739-747.
7. Pickup IM, McEnaney, B, Cooke RG. Carbon, 1986;24:535-543.
8. Neighbour GB, McEnaney, B. Carbon, 1994;32:553-558.
9. Kraus G, Semmler J. Carbon, 1978;16:185-190.
10. Andrew JF, Okada J, Wobschall DC. In Proc. 4th Conference on Carbon. New York:Pergamon. 1960:559-575.
11. Davidson HW, Losty HHW, Nature, 1958;181:1057-1059.
12. Sakai M, Urashima K, Inagaki, M. J. Amer. Ceram. Soc, 1983;66: 868-874.
13. Sakai M, Yoshimura J, Goto Y, Inagaki M. J. Amer. Ceram. Soc. 1988:71: 609-616.
14. Hartley M, McEnaney B. In Extended Abstracts 'Carbon '96', Newcastle upon Tyne: British Carbon Group. 1996:210-211.
15. Hartley M, McEnaney B. In Graphite moderator lifecycle behaviour. Vienna: International Atomic Energy Agency. IAEA-TECDOC-901. 1996:263-274.
16. Hartley M, McEnaney B. In Extended Abstracts of 23rd American Carbon Conference, Vol II. State College, PA: American Carbon Society, 1997: 228-229.

Figure 11. Optical micrographs of microstructural damage due to blunt indentation for three grades of graphite. a. Poco ZXF; b. Morganite EY306; c. BAEL IM1-24. 11 a,b, arrows indicate cone cracks; 11b, dashed line denotes limit of shear damage [15].